Available online at www.sciencedirect.com
SCIENCE DIRECT®
Thin Solid Films xx (2003) xxx–xxx
thin solid films
www.elsevier.com/locate/tsf

Analysis of laser-induced evaporation of Al target under conditions of vapour plasma formation

V.I. Mazhukin[a], V.V. Nossov[a], I. Smurov[b,*]

[a]*Institute of Mathematical Modelling of RAS, Miusskaya sqr 4a, 125047, Moscow, Russia*
[b]*I. Smurov, Ecole Nationale d'Ingénieurs de St-Etienne, 58 rue Jean Parot, 42023 St.-Etienne Cedex 2, France*

Abstract

The plasma-controlled evaporation of the Al target induced by the laser pulse with intensity of 10^9 W/cm^2 and wavelength of 1.06 μm is analysed with account for the two-dimensional effects. The self consistent model is applied, including the heat transfer equation in condensed medium, the equations of radiation gas dynamics in evaporated substance and the Knudsen layer model at the two media boundary. It is found that the phase transition at the target surface is controlled by the two factors: the surface temperature that depends on the transmitted radiation intensity, and the plasma pressure, governed by the expansion regime. The process comes through three characteristic stages, the sonic evaporation at the beginning, the condensation during the period of plasma formation and initial expansion, and finally, the re-start of evaporation in subsonic regime after the partial brightening of the plasma. During the subsonic evaporation stage the vapour flow and the mass removal rate are much higher near the beam boundaries than in the centre due to smaller plasma counter-pressure. The vapour plasma pattern is characterised by the dense hot zone near the surface where the absorption of laser energy occurs, and rapid decrease of density outside the zone due to three-dimensional expansion.

PACS: 68.10 Jy; 52.40Nk

Keywords: Laser-induced evaporation; Mach number; Laser plasma; Radiative gas dynamics; Stefan problem

1. Introduction

The evaporation of a matter induced by intensive laser radiation can proceed in two qualitatively different regimes depending on the temperature and pressure of near-surface heated region. If the temperature and (or) the pressure exceed critical values, the liquid–vapour transition is described by gas dynamic equations with the uniform equation of state [1]. In the opposite (sub-critical) case the process is characterised by sharp interface formation. The flux of evaporated matter is non-equilibrium, as all the vapour particles have velocity components in the direction away from the surface. For the sufficiently intensive evaporation the particles collide and develop equilibrium distribution over the distance of several free runs. The region adjacent to the interface, where the distribution transforms to the equilibrium one, is called the Knudsen layer (KL).

In terms of continuum mechanics the KL presents strong gas dynamic discontinuity [2–6], at which the mass, momentum and energy conservation are fulfilled. Also, additional relations are postulated that account for phase transformation kinetics and are derived by means of the different approximations of the distribution function inside the KL. The Mach number M defined at the outer boundary of the KL is widely used as the parameter characterising the degree of non-equilibrium (the intensity) of the evaporation. At $M=1$ the vapour flow through the surface reaches maximum and the process is maximum non-equilibrium. The $M=0$ condition means that the flow from the surface is equilibrated by the back-scattered flow, thus the total flow across the interface is zero and the two phases are in equilibrium. It is generally accepted that the normal velocity of the vapour flow at the outer side of the KL does not exceed

*Corresponding author. Tel.: +33-04-77-43-84-38; fax: +33-04-77-43-84-99.
E-mail address: smurov@enise.fr (I. Smurov).

0040-6090/03/$ - see front matter © 2003 Published by Elsevier B.V.
doi:10.1016/S0040-6090(03)01698-5

the local speed of sound and the $M>1$ regimes are not considered [2–4,7–10].

The laser-induced evaporation with $M=1$ takes place for irradiation in vacuum or low-pressure ambient atmosphere. In this case, heat transfer in the condensed medium is independent of vapour phase and is described by the single-phase version of the Stefan problem, with logarithmic dependence of the transition temperature on the front velocity [11,12]. For subsonic evaporation $0<M<1$ the description is much more complex because the processes in the condensed and vapour phases become coupled, the M parameter evolution is not known beforehand and it is determined in the course of solution [13]. The subsonic evaporation can be interpreted as controlled by the two factors: the thermal and gas dynamic ones, determined by the surface temperature and vapour pressure, respectively.

The unsteady regimes of laser evaporation were considered in a number of theoretical papers [14–21]. Several factors were established that can decelerate the process and reduce the M parameter: the environment back-pressure [14–16], the fast variation of the surface temperature [17–19] and the additional back-pressure of the vapour plasma [19–21].

The formation of plasma in the evaporated substance essentially complicates the laser/target interaction due to the sharp variation of the optical and thermal properties of the medium. The numerical analysis of the plasma-controlled laser evaporation was performed in several studies by means of one-dimensional in space (1D) [22–24] and two-dimensional (2D) [25–28] models. The screening effect of the laser plasma was predicted, however, the time development of the evaporation intensity (the Mach parameter) was not considered. This subject was addressed in Refs. [19–21] for the aluminium target evaporation in vacuum and the decisive role of the plasma pressure was established. The high pressure of the plasma not only decelerated but also reversed the direction of the phase transition, and the vapour began to condense on the surface despite the target temperature being approximately twice as high as the equilibrium boiling temperature. In the frame of 1D model two stages of evaporation were found: the first stage was induced by laser radiation ($M=1$); and the second one by the effect of plasma thermal radiation ($M\approx 0.1$).

The application of 2D model that is numerically much more cumbersome enables to derive additional information on evaporation process and, in particular, to establish the Mach number dependence on radial coordinate. The main objective of this paper is to analyse plasma-controlled evaporation induced by the laser pulse with the intensity of 10^9 W/cm^2 and the wavelength of 1.06 μm with account for 2D effects.

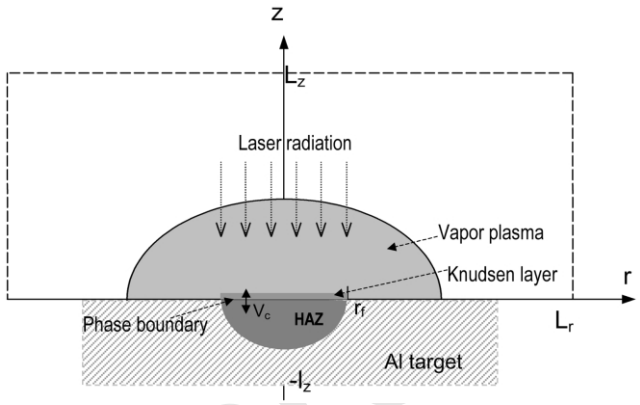

Fig. 1. Problem set-up.

2. Problem statement

The present 2D model consists of heat-transfer equation in condensed phase with Stefan type boundary condition at the irradiated surface, the set of equations of radiation gas dynamics and laser radiation transfer in vapour plasma, equations of state and absorption coefficient data. The principal assumptions are the following:

- Target melting and hydrodynamic phenomena in liquid phase are excluded from consideration. The melting has a minor influence on total energy balance because the latent heat of this process is much lower than that of evaporation. The melt hydrodynamics and related problem of solid and liquid macro-particles in the ablation plume are excluded due to the extreme complexity of corresponding mathematical models.
- The normal velocity of the vapour flow at the outer side of the KL is limited by the speed of sound for evaporation and condensation, $|M|\leq 1$.
- The plasma is treated as an absorbing medium in the state of local thermo-dynamic equilibrium and satisfies the quasi-neutrality condition; the plasma evolution is described in the approximation of a non-viscous non-thermoconducting gas.

For mathematical description moving cylindrical coordinate system is introduced with the origin fixed at the target surface in the laser beam centre, the r-axis directed along the surface and the z-axis directed along the outward normal (Fig. 1).

2.1. Condensed phase

Energy transfer in the condensed phase domain $0<$

$r<L_r$, $-l_z<z<L_z$ is governed by heat-conduction equation [29]:

$$\frac{\partial H_c}{\partial t}+V_c\frac{\partial H_c}{\partial z}=-\mathrm{div}\ \vec{W},\quad H_c=\rho_c C_p T_c,\ \vec{W}$$

$$=-\lambda\mathrm{grad}\ T_c \qquad (1)$$

Here 'c' index denotes the condensed phase, T_c, H_c, $\vec{W}$ are the temperature, volumetric enthalpy and heat flux, V_c is the surface recession velocity (interface velocity), ρ_c, C_p, λ are the density, specific heat and thermal conductivity. The external boundaries of the condensed domain are heat-insulated, with initial target temperature being $T_0=300$ K.

2.2. Gaseous phase and plasma

When the laser intensity is high enough, optical thickness of evaporated substance is sufficient to initiate an intensive absorption and avalanche ionisation. The resulting vapour plasma is partially or completely opaque for laser radiation. The work of pressure, laser energy release rate and the balance of plasma thermal radiation control its energy balance. In the vapour plasma domain $0<(r\times z)<(L_r\times L_z)$ the system of radiation gas dynamics (RGD) equations is written as follows [30,31]:

$$\frac{\partial\rho}{\partial t}+\mathrm{div}\ \rho\vec{V}=0 \qquad (2)$$

$$\frac{\partial\left(\rho\vec{V}\right)}{\partial t}+\rho\left(\vec{V}\cdot\mathrm{grad}\right)\vec{V}=-\mathrm{grad}\ P \qquad (3)$$

$$\frac{\partial\ (\rho e)}{\partial t}+\rho\mathrm{grad}\ e\vec{V}=-P\ \mathrm{div}\vec{V}-\mathrm{div}\vec{q}+\frac{\partial G}{\partial z} \qquad (4)$$

$$\mathrm{div}\vec{q}_\nu+\kappa_\nu U_\nu=\kappa_\nu U_{b\nu},\quad \vec{q}_\nu=-\frac{1}{3\kappa_\nu}\mathrm{grad}U_\nu,$$

$$U_{b\nu}=\frac{8\pi h\nu^3}{c^3\left(\exp\left(h\nu/kT\right)-1\right)},\quad \vec{q}=\int_\nu \vec{q}_\nu\,\mathrm{d}\nu \qquad (5)$$

$$P=P(\rho,T),\quad e=e(\rho,T)\quad \kappa_\nu=\kappa_\nu(\rho,T,\nu) \qquad (6)$$

where $\vec{V}=(u,\mathrm{v})$ is the gas-dynamic velocity, ρ, P, e are the density, pressure and volumetric internal energy respectively, $\vec{q}=(q_r,\quad q_z)$ is the radiative heat flux, κ_ν is the absorption coefficient of plasma radiation, U_ν, $U_{\nu,\mathrm{eq}}$ are the volumetric density of radiation and black-body radiation, 'ν' index denotes frequency dependent quantities. Eq. (5) describes radiation transfer in diffusion approximation [32]. The system of equations (Eqs. (2)–(6)) is supplemented by the boundary conditions Ref. [31]. The equations of state and absorption coefficient (Eq. (6)) are calculated by the technique of Ref. [33], which is based on the Hartree–Fock–Slater model.

Laser radiation transfer equation along the z-axis accounts for incident G^- and reflected G^+ components and is written within the laser beam domain $0<r<r_f$, where r_f is the beam radius:

$$\frac{\partial G^-}{\partial z}-\kappa G^-=0,\quad \frac{\partial G^+}{\partial z}+\kappa G^+=0,\quad G$$

$$=G^--G^+,\quad 0<z<L_z z=L_z{:}G^-$$

$$\equiv G_0,\quad z=L_z{:}G^+=(1-A(T))G^- \qquad (7)$$

where $A(T)$ denotes the surface absorptivity. The absorption coefficient of laser radiation κ for the 1.06 μm wavelength is determined by inverse Bremsstrahlung mechanism [32], and it is calculated assuming equilibrium charge composition.

2.3. Interface boundary conditions

The principal feature of evaporation problem is the presence of non-equilibrium domain adjacent to the surface, i.e. the Knudsen layer, in which the state of vapour cannot be described by continuous medium equations.

In general, vapour flow leaving the surface depends on the state of already evaporated substance above the surface, which is governed by gas-dynamic equations. The boundary conditions at the surface should link six quantities: the velocity V_c, the surface temperature T_c and pressure P_c, the vapour temperature, density and gas-dynamic velocity at the outer boundary of the Knudsen layer. For this purpose conservation of energy, mass and momentum is applied:

$$\lambda_c\frac{\partial T_c}{\partial z}=AG^-+L_v\rho_c V_c,\quad \rho_c V_c=\rho(V_c-\mathrm{v}),$$

$$\rho_c V_c^2+P_c=\rho(V_c-\mathrm{v})^2+P, \qquad (8)$$

as well as two additional relations, dependent on the applied approximation of Knudsen layer [7,8]:

$$\frac{T}{T_c}=\frac{2\gamma M^2(m^2+1/2)^2}{(1+\gamma M^2)^2m^2t^2},$$

$$\frac{\rho}{\rho_{\mathrm{sat}}}=\frac{tm^2(1+\gamma M^2)(\gamma M^2(m^2+1/2))^{-1}}{\exp(-m^2)+\pi^{1/2}m(1+\mathrm{erf}(\mathrm{m}))} \qquad (9)$$

Table 1
Thermo-physical and optical properties of aluminium

Variable	Value	Variable	Temperature dependence		
			$T_0=300$ K	$T_m=933$ K	$T_{cr}=8000$ K
T_b (K)	2720	λ (W/cm K)	2.37	0.75	0.16
P_b (Bar)	1.0	ρ (g/cm^3)	2.7	2.33	0.64
L_v (J/g)	1.1×10^4	C_p (J/gK)	0.95	1.2	1.2
A_m (g/mol)	27	A (%)	0.1	0.1	0.3

$$M=\mathrm{v}/\sqrt{\gamma RT},\quad \rho_{sat}=P_{sat}/(RT_c),$$

$$P_{sat}=P_b\exp\left(\frac{L_v}{RT_c}\left(1-\frac{T_b}{T_c}\right)\right),\quad R=\frac{R_0}{A}$$

$$f(m)=F(M)(m^2+1/2)^2-m^2(m^2+\alpha+3/2)=0, \qquad (10)$$

$$F(M)=1+\frac{3\gamma M^2-1}{\gamma M^2+1},\quad \alpha=2t^2-2^{-1}\pi^{1/2}mt-1,$$

$$t=\frac{2\,m}{\pi^{1/2}}+\frac{1+\mathrm{erf}(m)}{\exp(-\mathrm{m}^2)+\pi^{1/2}m(1+\mathrm{erf}(m))},$$

Here M is the Mach number, ρ_{sat}, P_{sat} are the saturated vapour density and pressure corresponding to surface temperature T_c, L_v is the latent heat of evaporation, R, R_0, A are the gas constant, universal gas constant and atomic mass, respectively, γ is the adiabatic constant equals to 5/3 for monatomic vapour, P_b, T_b are the pressure and equilibrium boiling temperature at the normal conditions.

The last undefined quantity (Mach number in the present case) is determined from the solution of gas-dynamic equations. While M is found, the quantities m, t, α necessary to evaluate the relations (Eq. (9)) are found by solving non-linear Eq. (10). At $M=0$ the evaporation (convective) is absent, the total vapour flow across the boundary is equal to zero, the temperature is continuous and the vapour above the surface is in saturated state. At $M>0$ temperature, density and pressure of vapour are discontinuous, with maximum deviation reached at $M=1$, sonic evaporation: $T=0.633\,T_c$, $\rho=0.326\rho_{sat}$, $P=0.203P_{sat}$. The flow of evaporated substance in this case also reaches maximum equal to 0.825 of Herz–Knudsen flow $j_{HK}=\rho_{sat}\sqrt{RT_c/2\pi}$.

If $P_{sat}<P$ relation is fulfilled at the Knudsen layer ($M<0$), then the evaporation turns into condensation. According to the results of numerical and analytical studies [10,34–36], only one condition is imposed on the three quantities T/T_c, M and ρ/ρ_{sat} (or P/P_{sat}) in the case of subsonic condensation, for example $\rho/\rho_{sat}=F_1(T/T_c, M)$, $P/P_{sat}=F_2(T/T_c, M)$, while the values of the other two parameters T/T_c and M are controlled by the state of gas dynamic flow. At present, the analytic expressions for F_1, F_2 functions are derived only for several limited cases, and in general they are determined numerically from the solution of Boltzmann equation and tabulated. The results of Ref. [35] are used in the present model for $P/P_{sat}=F_2(T/T_c, M)$ relation. F_2 has only weak dependence on temperature and is approximated as $P/P_{sat}\approx F^*(M)\approx 0.95\exp(2.42\,M)$. In opposite to evaporation, the condensation can proceed in supersonic regime, which is characterised by the modified set of boundary conditions as compared to the subsonic condensation [10].

2.4. Numerical algorithms

The differential problem (1)–(10) is solved by finite – difference (FD) technique. The computational grid along the r-axis in the $0<r<L_r=5$ cm domain consists of 50–100 nodes and it is more dense in the laser action zone $0<r<r_f$. The non-uniform grid along the z-axis is constructed separately in condensed ($l_z=0.01$ cm, 40 nodes) and gaseous ($L_z=10$ cm, 100–200 nodes) domains. The smallest grid steps are at the target surface and are equal to 2×10^{-6} cm and 10^{-5} cm for condensed and gaseous phases, respectively. The non-linear heat transfer equation with convective term is approximated by implicit FD equation using five-point stencil [37]. The equation was solved by alternative direction method. The FD approximation and computational algorithms applied for RGD part of the model are described in detail in Ref. [38]. The algorithm for the whole problem consists of the following three blocks: (1) the solution of RGD equations; (2) the evaluation of boundary conditions; (3) the solution of heat transfer equation that is iteratively executed at each time step [21].

3. Results and discussion

Consider processes at Al target surface irradiated by the laser pulse with intensity of 10^9 W/cm^2, 'tophat' spatial profile and rectangular pulse shape, with wavelength $\lambda=1.06$ μm, beam radius $r_f=0.025$ cm and pulse duration of 100 ns. Thermo-physical and optical properties of Al used in computations are presented in Table 1.

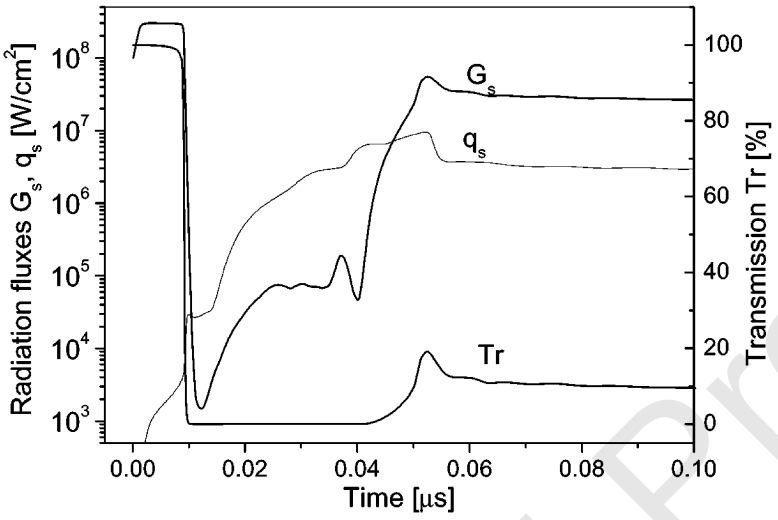

Fig. 2. Transmitted laser intensity G_s, transmission coefficient Tr and radiative heat flux q_s vs. time at $r=0$, $z=0$.

3.1. The processes in the beam centre

The intensity of laser radiation reaching the target is the principal parameter governing the processes on the surface. The evolution of absorbed intensity in the beam centre $G_s=AG^-(r=0,\ z=0)$, as well as vapour plasma transmission coefficient along the beam axis $Tr=G^-(r=0,\ z=0)/G_0$ are presented in Fig. 2. At the beginning of laser pulse the evaporated substance above the surface is transparent and all the laser energy reaches the surface: $Tr=100\%$, $G_s=AG_0=3\times10^8$ W/cm^2. The evolution of the process changes qualitatively when plasma is formed in the vapour. The plasma effectively absorbs the laser radiation due to high electron concentration and the laser action on the surface terminates, Fig. 2: $G_s\approx10^3$ W/cm^2, $Tr\approx0$. Later on as the plasma expands, it becomes partially transparent and starting from $t\approx50$ ns the transmission coefficient remains at approximately constant level $Tr\approx10\%$, $G_s\approx3\times10^7$ W/cm^2.

Let's return now to the main subject of the present analysis—the phase transformation of the surface. The process is characterised by the following quantities taken at the beam centre $r=0$: surface temperature T_c, Mach number M, Fig. 3, saturated vapour pressure P_{sat} and vapour plasma pressure P_p, Fig. 4. As indicated in Fig. 3, three specific stages of the process are distinguished. Intensive laser energy release in near-surface layer courses its fast heating and in a short time the vapour flow reaches the sound velocity ($M=1$), therefore in further consideration the stage I will be referred to as sonic evaporation. However, both the surface temperature and, as a consequence, the vapour flow velocity continue to increase. Steady-state evaporation regime is reached over

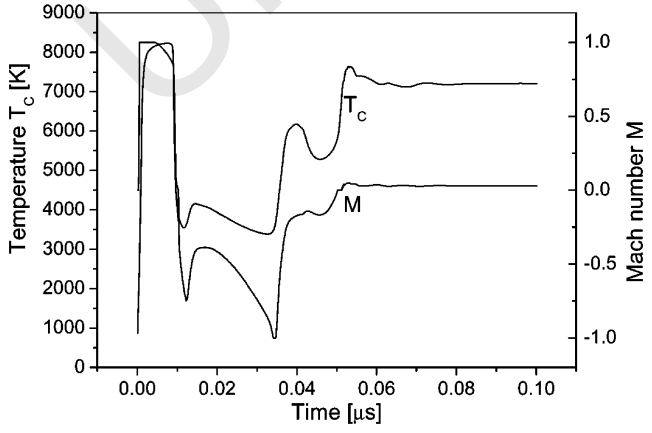

Fig. 3. Target surface temperature T_c and Mach number M vs. time at $r=0$, $z=0$.

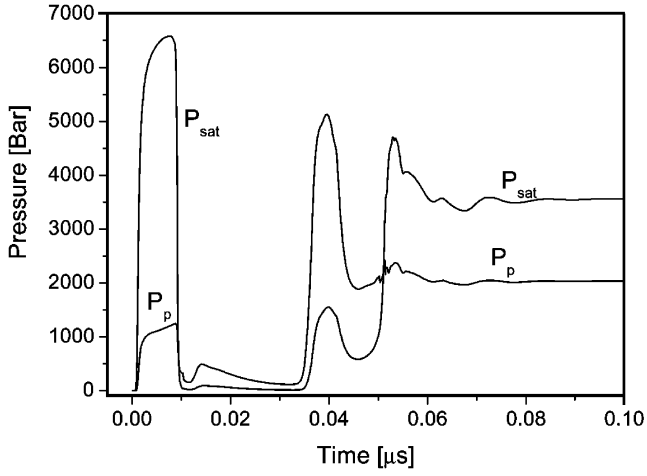

Fig. 4. Saturated vapour pressure P_{sat} and plasma pressure P_p vs. time at the beam centre.

2–3 ns with the surface temperature close to the critical point; it is characterised by the equality of laser energy input G_s and the energy losses due to evaporation and conductive heat flux $-\lambda\ \mathrm{grad}(T_c)$ toward the bulk of the target. As seen in Fig. 4, the condition $P_{sat} > P_p$ is fulfilled during the stage I: saturated vapour pressure is approximately five times higher than the plasma pressure.

After the plasma formation the energy input to the target surface is terminated, its temperature and saturated vapour pressure are rapidly diminished, at $t \approx 12$ ns the $P_{sat} < P_p$ condition is realised and evaporation turns to condensation, Figs. 3 and 4, stage II, $M < 0$. Majority of time the condensation proceeds in subsonic regime. The Mach number sharply decreases and reaches the 1 value at $t \approx 40$ ns, when disturbance from the plasma initial ignition region reaches the surface (see the peak of the P_p curve in Fig. 4).

High pressure of the plasma results in its rapid expansion. As vapour flow from the surface to plasma is absent, the expansion leads to the partial restoration of transparency and the onset of subsonic evaporation stage, Figs. 3 and 4, stage III, with very low Mach number close to the boundary of convective evaporation $M \approx 0.05$ [4]. The comparison of evaporation at the stages I and III gives insight into the relation of temperature and gas-dynamic factors—temperature and saturated vapour pressure on the stage III are only slightly lower than that of the stage I, Figs. 3 and 4 however, the flow is decelerated by strong plasma counter-pressure. It is worth to mention that due to small Mach number the vapour density at the stage III is just as high as saturated vapour density $\rho(M = 0.05) \approx 0.95\rho_s$ and exceeds the vapour density at the stage I $\rho(M = 1) = 0.32\rho_s$.

The effect of plasma thermal radiation is illustrated by the radiation flux reaching the surface in the beam centre $q_s = q_z(r = 0,\ z = 0)$, Fig. 2. At the stage II the plasma radiation is as high as 10^7 W/cm^2 and it keeps the surface at relatively high temperature. At the stage III the plasma radiation flux is $\approx 3 \times 10^6$ that is one order of magnitude lower than the laser intensity.

3.2. Plasma pattern structure

Consider some features of plasma pattern evolution that essentially influence the surface phase transformation. The plasma temperature profiles along the z-axis taken at several instants are presented in Fig. 5. Initially plasma is formed at the forefront of the vapour cloud at the distance of $\approx 10^{-2}$ cm from the surface, Fig. 5, 20 ns. Later on the plasma expands rapidly in two opposite directions—towards the laser source and towards the surface. At $t = 40$ ns the ionisation front reaches the surface, and this event manifests itself as a peak of

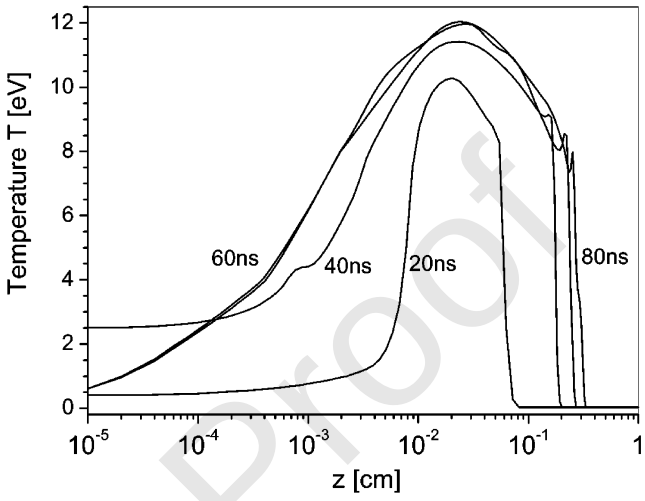

Fig. 5. Plasma temperature profiles at the beam axis.

temperature and pressure in Figs. 2 and 4. Starting from 60 ns the temperature profiles of steady shape slowly propagate in positive z-direction.

Contour plots of 2D temperature distributions taken at $t = 20$ ns and $t = 70$ ns are presented in Fig. 6. The Fig. 6a and the curve '20 ns' in Fig. 5 represent the same plasma plume. It is found that radial expansion of the plume is rather limited at this instant. The instant 70 ns, Fig. 6b corresponds to steady expansion regime that is characterised by the axial expansion velocity being two times as high as the radial one. The plasma hot core is situated near the surface where laser energy release takes place with the local temperature maximum at the forefront. Density distribution at $t = 70$ ns is shown in Fig. 7. It is characterised by rapid density decrease with the distance from the surface. Starting from 10^{-1} g/cm^3 at the Knudsen layer the density lowers down to 10^{-3} g/cm^3 at the distance of 5×10^{-3} cm, to 10^{-4} g/cm^3 at the distance of 4×10^{-2} cm and 10^{-5} g/cm^3 at 0.1 cm. It confirms an obvious fact that in $z < \approx r_f$ domain the density follows $\sim 1/z$ law and varies as $\sim 1/z^3$ at larger distance. Therefore, despite the high temperature of the plasma cloud its major part remains transparent for laser radiation.

The location of laser energy absorption zone is an important feature of the plasma pattern, (Fig. 8), $G^-(z,\ r = 0)$. At $t = 20$ ns energy release takes place in the narrow region around $z \approx 10^{-2}$ cm. Further on, the absorption zone becomes wider and the energy release rate $\partial G/\partial z$ diminishes.

3.3. Processes on the surface

Analysis of phase transition in the Section 3.1 is related to only one point at the beam centre, i.e. it is quasi-one dimensional. The evolution of target temper-

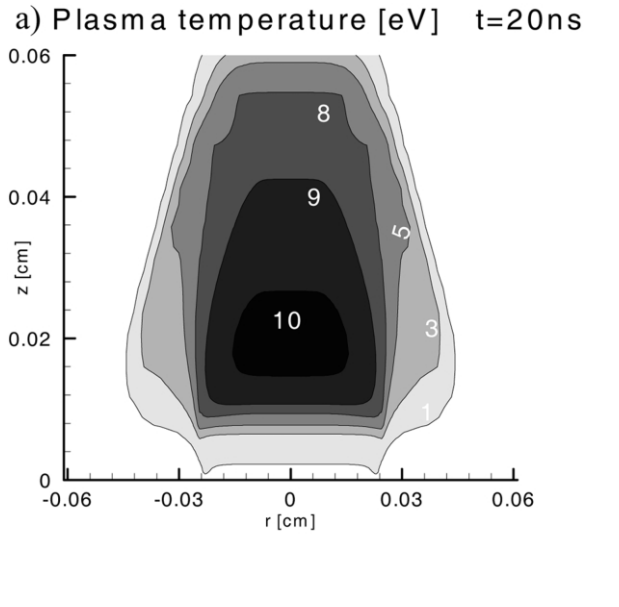

Fig. 6. Contour plot of the plasma temperature at $t=20$ ns: (a) and $t=70$ ns: (b).

ature profiles, $T_c(r, z=0)$, is presented in Fig. 9. At $t=8$ ns the plasma in vapour phase has not yet formed and the temperature across the irradiation zone $|r|<r_f$ is constant. The profile at $t=10$ ns already corresponds to plasma–mediated action. Comparison of the two curves shows that for over 2 ns the temperature is dropping sharply everywhere (due to evaporation heat losses), except for the narrow zone near the beam boundary. The profiles at later instants correspond to the condensation stage and demonstrate that the recommence of evaporation starts near the beam edges and later on with 10–20 ns shift in the central zone. This fact indicates that the plasma brightening is not only the result of axial plasma expansion but its lateral expansion as well. The latter effect manifests itself earlier at greater distance from the beam centre. Starting from $t=60$ ns the surface temperature becomes practically uniform over the laser spot.

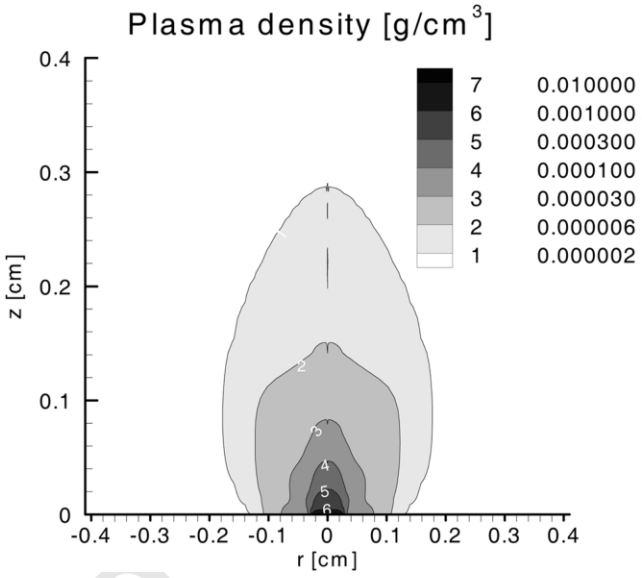

Fig. 7. Contour plot of plasma density at $t=70$ ns.

Radial expansion reduces the plasma counter-pressure near the boundaries of evaporation zone, so hypothetically the mass removal should be more intensive there. The assumption is confirmed by the results presented in Fig. 10 showing the evolution of Mach number at the surface for three specific radial points: $r=0$, $r=r_f/2$ and $r=r_f$. The processes in the former two points goes on identically, but at the beam boundary the re-start of evaporation occurs earlier and the vapour flow velocity, characterised by the Mach number, is several times higher than in the centre.

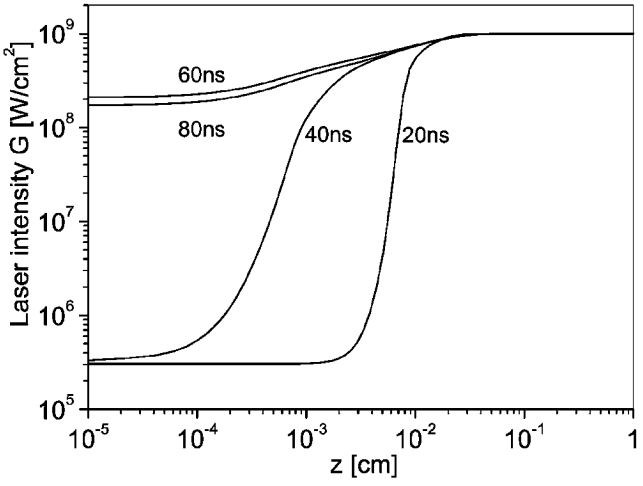

Fig. 8. Incident laser intensity profiles at the beam axis.

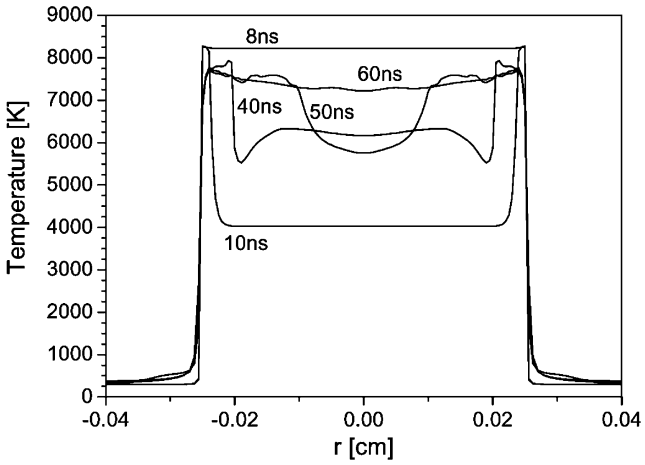

Fig. 9. Surface temperature profiles vs. radius.

The amount of the removed material vs. radius is presented in Fig. 11. It is calculated by integration the surface recession velocity. The curve taken at $t=10$ ns shows that just before the plasma ignition the removed layer has constant thickness. Over the next 30 ns it partially decreases due to vapour condensation. Well seen circular hollow near the beam edge at $t=40$ ns and especially at 100 ns indicates that this part of evaporation zone gives significant contribution to the total amount of evaporated material. Note that the results presented in Fig. 11 cannot be interpreted as profile of laser crater because melting and melt hydrodynamics are excluded from the present analysis.

4. Conclusion

The performed studies allow to draw the following conclusions on phase transition of Al surface induced by laser radiation with the intensity of 10^9 W/cm^2, the wavelength of 1.06 μm and the beam radius of 0.025 cm:

- Phase transition of the target surface is controlled by the two factors: the surface temperature that depends on transmitted radiation intensity and the plasma pressure, governed by the expansion regime. The process comes through three characteristics stages—the sonic evaporation at the beginning, the condensation during the period of plasma formation and initial expansion and, finally, the re-start of evaporation in subsonic regime after the partial brightening of the plasma.
- During the subsonic evaporation stage the vapour flow and the mass removal rate are much higher near the beam boundary than in its centre due to smaller plasma counter-pressure, therefore it is just the 'periphery' part of the irradiation zone that gives the significant contribution to the total amount of removed material.
- The vapour plasma pattern is characterised by the dense hot zone near the surface at the distance of an order of the beam radius where the absorption of laser energy takes place, and rapid decrease of density outside the zone due to three-dimensional expansion.

The predicted results characterise the specific features of laser-induced plasma-mediated ablation, and provide information potentially useful for the development and improvement of pulsed laser deposition (PLD) technique. However the analysed regime of laser action differs from typical PLD applications that utilise eximer lasers with the wavelength in the ultraviolet range, shorter (≈20–30 ns) pulses and lower fluency. It is planed to continue this study and to extend the analysis for typical PLD conditions.

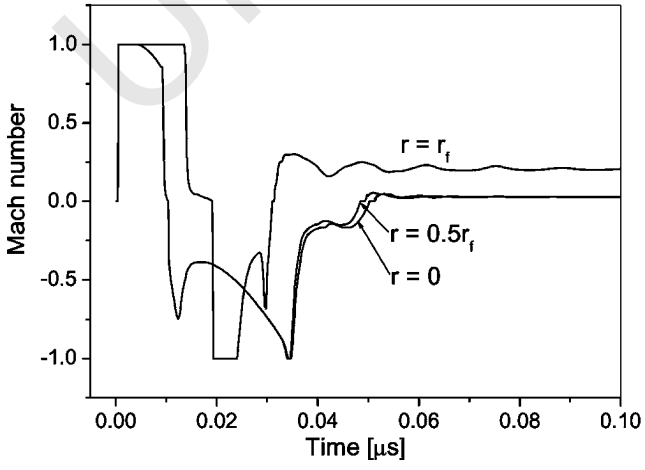

Fig. 10. Mach number evolution at different radial points.

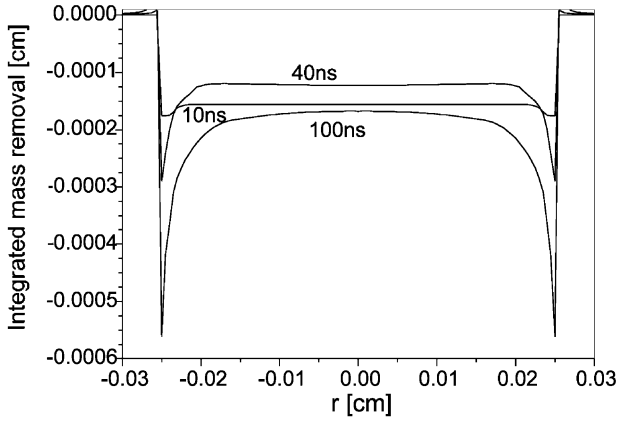

Fig. 11. Total mass removal vs. radius.

References

[1] Yu.V. Afanasiev, O.N. Krokhin, in: P. Kalderola, G. Knopfel (Eds.), Fizika Visokikh Plotnostej Energij, Mir, Moskva, 1974.

[2] G.S. Romanov, V.K. Pustovalov, Izvestia AN BSSR Serija Fiz. Mat. 4 (1967) 84.
[3] S.I. Anisimov, Sov. Phys. JETP 27 (1968) 182.
[4] Ch.J. Knight, AIAA J. 17 (1979) 519.
[5] A.A. Samokhin, Sobshchenija po Fizike FIAN 6 (1982) 3.
[6] B.Ya. Mojzhes, V.A. Nemchinskii, J. Tekh. Fiz. 52 (1982) 684.
[7] D. Crout, J. Math. Phys. 15 (1936) 1.
[8] V.I. Mazhukin, P.A. Prudkovskii, A.A. Samokhin, J. Mat. Modelirovanije 5 (1993) 3.
[9] M. Aden, E. Beyer, R. Herziger, J. Phys. D: Appl. Phys. 23 (1990) 655.
[10] Y. Sone, S. Takata, F. Golse, Phys. Fluids 13 (2001) 324.
[11] Masters, J. Appl. Phys. 27 (1956) 477.
[12] A.A. Samokhin, Effect of laser radiation on absorbing condensed matter, In: A.V. Prokhorov (Ed.), Proceedings of General Physics Institute USSR Academy of Science, vol. 13, Nova Science, New York, 1990.
[13] V.I. Mazhukin, A.A. Samokhin, Dokl. Akad. Nauk. SSSR 281 (1985) 830.
[14] P.V. Breslavskii, V.I. Mazhukin, Preprint of All Union Centre of Math. Modelling 2 (1992) 1.
[15] S.H. Jeong, R. Greif, R.E. Russo, Appl. Surf. Sci. 129–127 (1998) 177.
[16] A.V. Gusarov, A.G. Gnedovets, I. Smurov, J. Appl. Phys. 88 (2000) 4352.
[17] Ch.J. Knight, AIAA J. 20 (1982) 950.
[18] V.I. Mazhukin, A.A. Samokhin, Sov. J. Quant. Electron. 12 (1985) 2432.
[19] V.I. Mazhukin, A.A. Samarskii, Surv. Math. Ind. 4 (1994) 85.
[20] V.I. Mazhukin, G.A. Pestryakova, Dokl. Akad. Nauk. SSSR 278 (1984) 843.
[21] V.I. Mazhukin, G.A. Pestryakova, J. Vichislitelnoj Mat. Mat. Fiz. 25 (1985) 1697.
[22] V. Bergelson, I. Nemchinov, Sov. J. Quant. Electron. 8 (1978) 1198.
[23] C. Phipps, R. Dreyfus, in: A. Vertes, R. Gijbels, F. Adams (Eds.), Laser Microprobe Mass Analysis, John Wiley and Sons, New-York, 1993.
[24] A. Vertes, R.W. Dreyfus, D.E. Platt, IBM J. Res. Dev. 38 (1994) 3.
[25] G.S. Romanov, Yu.A. Stankevich, Fiz. i Khimija Obrabotki Materialov 4 (1981) 15.
[26] V.I. Zubov, V.M. Krivtsov, I.N. Naumova, Yu.D. Shmiglevskii, J. Vich. Mat i Mat. Fiz. 23 (1983) 1520.
[27] M. Aden, E.W. Kreutz, A. Voss, J. Phys. D: Appl. Phys. 25 (1993) 1545.
[28] J.R. Ho, C.P. Grogoropoulos, J. Appl. Phys. 78 (1995) 4696.
[29] H.S. Carslaw, J.G. Jaeger, Conduction of Heat in Solids, Clarendon, Oxford, 1959.
[30] B.N. Chetveruskin, Dinamika Izluchajushchego Gaz, Mir, Moskva, 1992.
[31] V.I. Mazhukin, V.V. Nossov, I. Smurov, J. Appl. Phys. 90 (2001) 607.
[32] Ya.B. Zeldovich, Yu.P. Raizer, Physics of Shock Waves and High Temperature Hydrodynamics Phenomena I, Academic, New York, 1967.
[33] G.S. Romanov, Yu.A. Stankevich, K.L. Stepanov, Int. J. Heat Mass Transfer 38 (1995) 545.
[34] A.P. Kryukov, Heat Transfer Res. 24 (1992) 984.
[35] K. Aoki, Y. Sone, T. Yamada, Phys. Fluids A 2 (1990) 1867.
[36] A.V. Gusarov, I. Smurov, 14 (2002) 4242.
[37] A.A. Samarskii, Teorija Raznostnikh Schem, Nauka, Moskva, 1992.
[38] V.I. Mazhukin, I. Smurov, G. Flamant, J. Comp. Phys. 112 (1994) 78.